AIRBORNE MEASUREMENT – ADVANCED INSTRUMENT DEVELOPMENT METHODS AND INSIGHT

#NJ Lawson[1]
[1]National Flying Laboratory Centre, School of Aerospace, Transport and Manufacturing, Cranfield University, Cranfield MK43 0AL, U.K.

Corresponding author; n.lawson@cranfield.ac.uk

Abstract— Airborne measurement is required in many fields of aerospace, ranging from aircraft development and flight test, to atmospheric sciences. It involves the use of aircraft mounted instruments to measure quantities ranging from simple parameters such as pressure and airspeed, to more complex quantities such as atmospheric aerosols and solids. Although well-established traditional methods are available to design instruments in the airborne environment, the application of new advanced methods and sensors to refine instrument design, has seen slow adoption by most of these fields. The following paper presents examples of new approaches, which are used to refine a number of airborne instruments, including the measurement of sideslip angle and angle of attack using traditional instruments and strain and pressure using advanced fibre optic sensors. An example of the application of these methods to aerosol measurement is also discussed. In most cases, it is concluded instruments can be readily and quickly refined using these new techniques, including computational fluid dynamics. New sensors also offer potential improvements in the measurement of many airborne measurands.

Keywords - airborne sensor test, CFD, fibre optic sensor

I. INTRODUCTION

Airborne measurement is a critical requirement in the design and testing of aircraft and it still relies on traditional methods including pressure and vane measurement (Wuest 1980; van der Linden and Mensink 1977). It also plays a vital role in the field of airborne science where bespoke instruments are typically mounted on the fuselage or wings of an aircraft (McBeath 2014).

In a typical aircraft instrument, which may measure critical items such as airspeed or altitude, corrections are applied to the basic instrument to ensure the required levels of accuracy are met in flight (Reasor et al 2015). However, in some cases in airborne test platforms, limitations on where the instrument can be fitted can lead to undesirable performance of the instruments and specialised corrections are generally required (Bennett et a1 2017a; Bennett et al 2017b).

In the last 20 years, computational fluid dynamics (CFD) has seen rapid development in the aerospace sector

(Anderson 1995; Jameson & Ou 2011; Lawson et al 2017). This has allowed complex corrections to be applied to airborne instruments by using the CFD model of the full aircraft and instrument installation along with flight test data (Lawson et al 2013; Lawson et al 2014; Bennett et a1 2017a; Bennett et al 2017b; Reasor et al 2015).

Further advancements in sensor technology are also now offering new opportunities in airborne test and aircraft design (Boden et al 2013). In particular fibre optic sensors

which can measure pressure (Rao 2006), strain (Rao 1999) and displacement (Kissinger 2018) have been applied to a number of airborne platforms and offer a number of advantages including their footprint, resolution and installation (Lawson et al 2016, Lawson et al 2017, Bennett and Lawson 2018)

The following paper presents examples of the application of CFD to airborne instrument development and also presents example of applications of advanced fibre optic sensors to airborne measurement.

PREPARATION OF THE MODELS

A key part of the process in modelling the airborne test system is to obtain a fully scaled CFD model. In nearly all cases, a solid model will not be available to generate the CFD solution. Original Equipment Manufacturers (OEMs) do not release this data except with significant restrictions or unless the intellectual property output during the project was protected. Also many airborne research platforms are old airframes and are likely to have been designed without access or with limited access to computer aided design (CAD).

Therefore the best approach in these circumstances is to generate the solid model from a laser scan of the aircraft. Not only does this method ensure a full scale solid model is obtained, but it also ensures that any features which are key to the airborne platform, e.g. pods or blisters or other mounts, are also captured in the solid model. A typical process required to obtain a solid model is outlined below in Figure 1.

In the first stage of the process, the aircraft must be prepared before scanning to ensure the minimum number of changes to the solid model following the scan. So for example, the ideal situation is to have all the instruments on the aircraft that which correspond to the airborne test.

Also the instruments must ideally be configured in the same condition as expected for the test. Control surfaces must be set to typical flight angles as they may also have an impact on the flow field around the instruments.

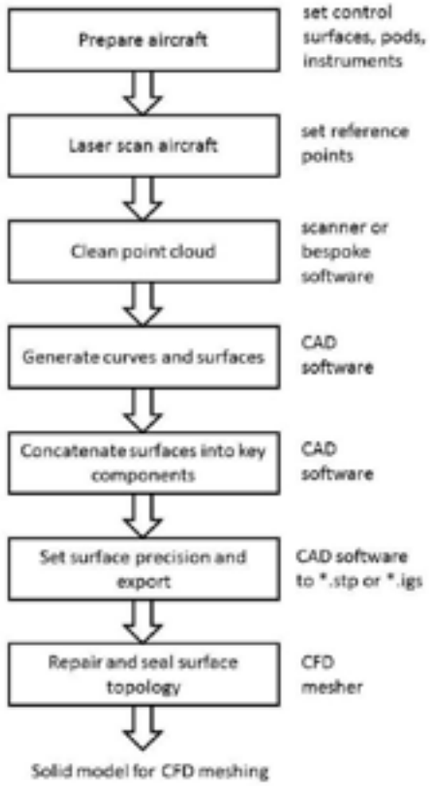

Figure 1. Process used to obtain a solid model for CFD from an airborne test airframe

During the scanning process, a further consideration is the position of reference points or mirrors for the scanner. Generally the laser scanner systems rely on photogrammetric reconstruction and a number of reference points in 3D space are required around the aircraft. For larger aircraft, this may require a greater volume than the hangar space available or where the aircraft is stored. In this situation, the aircraft must be scanned outside. There can also sometimes be issues with windows and canopies on the aircraft as the scanner will not receive a reflected signal. In these circumstances, all windows on the aircraft may need preparing with a removable powder or paint, which does not compromise the integrity of the window materials. Typically due to the optics of the scanner, the resolution of the scanner is fixed as a percentage of the range of distances being scanned. Hence, larger aircraft will result with larger absolute errors in the scanned geometry, but for the purposes of the CFD model, unless an instrument is positioned in a critical area, such as a transition region, these small geometric errors can be tolerated in the overall model.

Following the laser scan, the output is generally in the form of a point cloud which must be cleaned and prepared for export. In some situations, an assumption about the aircraft geometry is made and only half the aircraft is scanned with the point cloud being reflected about a reference line, before export to the CAD software.

Once the point cloud is imported into the CAD software, unless bespoke or specialised functions are available, surfaces must be individually generated by the CAD user by selecting areas of the point clouds to define curves. This reduced functionality can be found with academic licences for software such as CATIA or AutoCAD. If the point cloud is imported directly into the CFD meshing software, this can also cause issues as it is harder to control the surface mesh characteristics with this kind of approach. Therefore the selection and definition of curves is a time consuming process and is open to interpretation by the CAD user, to ensure a representative set of surfaces are prepared. Generally when this process is complete, to ensure fidelity of the overall surface model, there will be a significant number of surfaces which will need concatenation into less, key surfaces for the solid model, for example the fuselage, the wing top and bottom and the tail plane surfaces. At this stage, it is also important that the instrumentation under study for the model has sufficient fidelity, to ensure the local flow physics around the instrument is captured. In the author's experience, concatenation functions on most common CAD packages will provide a good reduced surface model for the CFD.

In the final stage of the CAD preparation, a suitable tolerance must be set for the export of the model into either IGES or STEP format. If these tolerances are not set correctly, when the CAD data is imported into the CFD meshing software, gaps will exist between some of the surfaces which will cause issues with the meshing. Providing these holes or gaps are not substantial, most meshing software such as Ansys ICEM CFDTM can automatically repair these holes using basic topology functions.

The following sections will now describe examples of the application of solid and CFD models to the design and refinement of airborne test instrumentation. For the Bulldog and BAE146 aircraft, a Leica ScanStation 2 was used with Leica Cyclone software to obtain the point cloud to develop the solid models.

BULLDOG AIRBORNE TEST MODEL

In the following example, a design of air data boom is modelled on the Bulldog wing by using CFD. To simplify the modification, the boom is mounted off the leading edge of the port wing with the sideslip angle and angle of attack vanes positioned less than one wing chord away from the leading edge (See Figure 2). This vane position results in a measurement error due to the effect of the upwash of the wing. The most significant error is in angle of attack and at higher angles of attack near the stall.

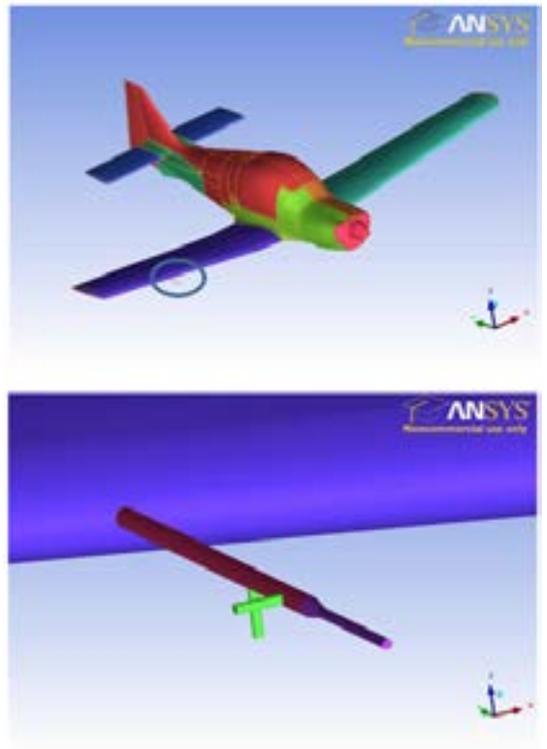

Figure 2. A CAD view of the air data boom on a Bulldog aircraft

As shown in Figure 2, the boom geometry is carefully modelled up to the vane and the flow characterised at the vane position through a range of angles of attack and sideslip. Here each vane is assumed to follow the local flow component and therefore the vane itself is omitted from the geometric model. This approach not only simplifies the CAD solid model but also simplifies the CFD mesh adjacent to the vanes.

In this case, the mesh and an example of the solution are shown in Figure 3. The effect of the upwash on the vane region of the databoom is clearly seen.

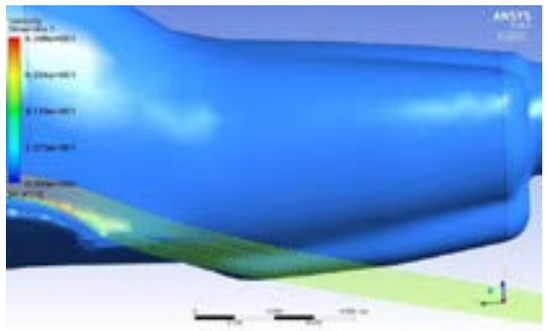

Figure 3. A CFD solution of the air flow over the data boom on a Bulldog aircraft

The results successfully characterise the upwash angle over the test conditions before the stall. Validation of the CFD is through previous published generic charts of upwash angle generated by potential flow solutions and modified lifting line methods outlined by Rawlings (1981). Figures 4 - 6 shows the CFD results predict the measured angle of attack as double the true value, where the measurement of sideslip angle show negligible error over the full range of angle of attack or sideslip angle measured. Further results show an improvement in the error when extending the boom position away from the leading edge and a degradation of error when positioning the boom closer to the leading edge. From this modelling, functions can then be developed which predict the error throughout the range of boom conditions and these functions can be incorporated into the measurement process to correct the data either during or after the flight test campaign.

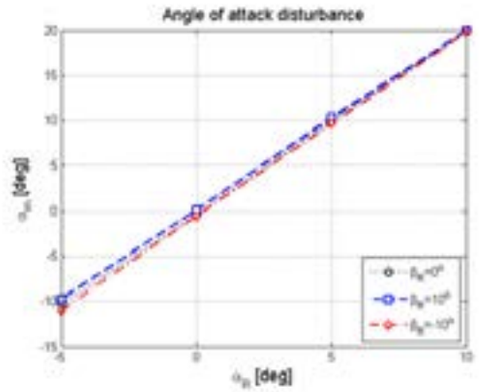

Figure 4. Effect of upwash on the measured angle of attack on the Bulldog air data boom over a range of sideslip angles

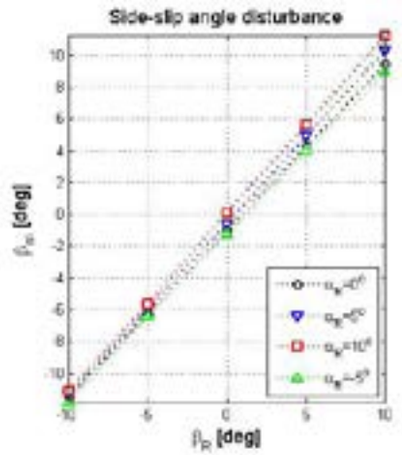

Figure 5. Effect of upwash on the measured angle of sideslip on the Bulldog air data boom over a range of sideslip angles

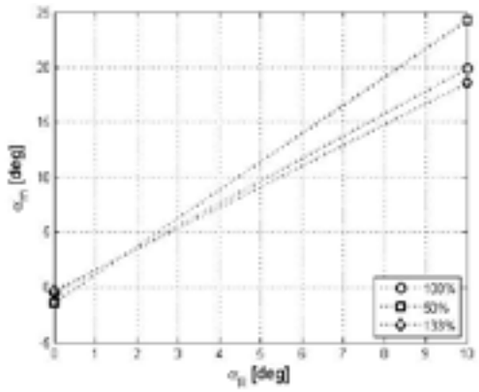

Figure 6. Effect of air data boom position on the measured angle of angle on the Bulldog data boom at zero sideslip angle

From this CFD data a calibration model can be developed based on linear behaviour which takes the form:

$$(\ , \ ) = (\ , \ ) + (\ , \ ) \qquad (1)$$

where is the real angle of attack, m is the measured angle of attack, m is the measured sideslip angle, k is the angle of attack calibration coefficient and k is the sideslip calibration coefficient.

IV. JETSTREAM AIRBORNE TEST MODEL

A further example of the application of CFD to minimise instrument measurement errors involves the development of a detailed model of a set of sideslip vanes and angle of attack vanes, positioned on the nose of the Cranfield University Jetstream aircraft. In this case, to simplify the certification process, the set of vanes were installed on the top and side of the aircraft nose and a flight test was used to estimate the vane angle characteristics (See Figure 7). The CFD mesh for the model is also shown below where the refined mesh around three vane positions can be seen (Figure 8).

The CFD model of the nose region, which also included an angle of attack vane, allowed characterisation of the vane angles through a matrix of flight conditions. In the figure below (Figure 9), which shows the local streamlines in the region of the nose, it is clear the presence of the nose is inducing an error between the true angle of attack, defined through the far field and the measured angle of attack defined by the local streamline.

This relationship also depends on sideslip angle and vice-versa. Therefore using the range of range of angle of attack and sideslip simulated in the CFD model, a relationship can be developed between angle of attack and sideslip angle as measured by the three vanes and the true sideslip and angle of attack that the aircraft was flying.

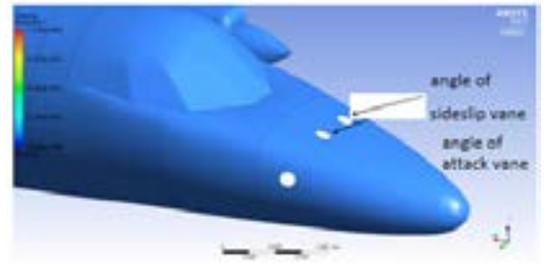

Figure 7. Jetstream 31 angle of attack and sideslip vane installation

Figure 8. Jetstream 31 angle of attack and sideslip vane CFD mesh

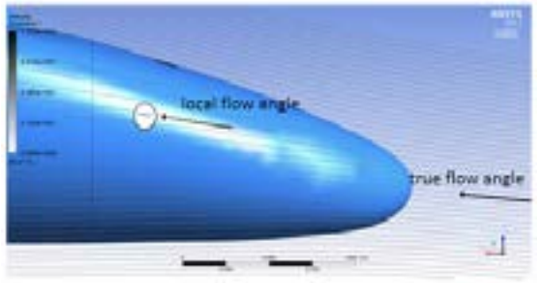

Figure 9. Jetstream 31 flow visualisation in the vane region showing the difference in true and measured angle of attack

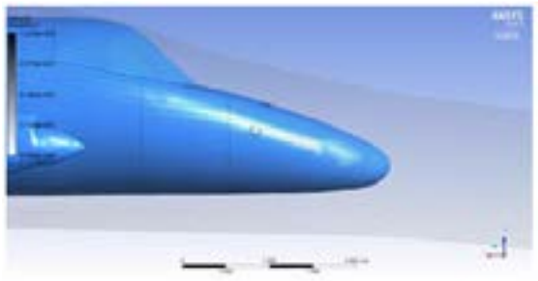

Figure 10. Jetstream 31 flow visualisation in the vane region

Using this relationship, a true angle of attack and sideslip for any flight condition can be estimated under any flight condition. This CFD model of the nose vanes was then checked using independent flight test data taken from an inertial reference unit mounted inside the aircraft.

As the modelled system now uses three measured sources to estimate two true values, a more complex relationship is used which takes the form:

the fan face and the flow conditions at the nearest canisters studied with and without the jet. In this case no significant changes in local pressure coefficient or flow angle were found and so the remaining solutions used empty nacelles.

= +13+22+3+4 53+62+7+8 (2)

= +93+102+11+12 133+142+15+16 (3)

= +173+182+19+20 213+222+23+24 (4)

where the constants k1 – k24 are obtained through correlations of the CFD data and flight test data. Therefore for any value of m or m, the equations can be solved to yield the true values and from the vane data.

V. BAE146 AIRBORNE TEST MODEL

A final example of the application of CFD to study instrument installation effects was the development of a detailed model of the wing booms found on the Facility for Airborne Atmospheric Measurement (FAAM), which is a BAE Systems 146 aircraft (McBeath 2014). This aircraft has been fitted with underwing pods on the outboard section of each wing. Each underwing pod contain 4 standard particle measuring Systems (PMS) sized canisters which allows the aircraft to carry a range of atmospheric sampling instruments.

A full scan of the aircraft was undertaken using the Leica ScanStation2 and as outlined previously a solid model was developed for meshing in ICEM CFD. The solid model from this process, which includes the canisters in a basic configuration, is shown in Figure 10.

The CFD solutions studied were both viscid and inviscid and with and without the influence of the jet engines in the nacelles. In the former case, viscid and inviscid models showed little difference in the behaviour of the local flow around the canisters due to the high Reynolds numbers of the airborne test conditions. Therefore inviscid models were chosen for the remaining study to save computational time and resources. With inclusion of the jets, there was concern that the engines would influence the local flow around the most adjacent canisters. Therefore a representative pressure ratio and mass flow was set up in the nacelle as a pressure jump condition at

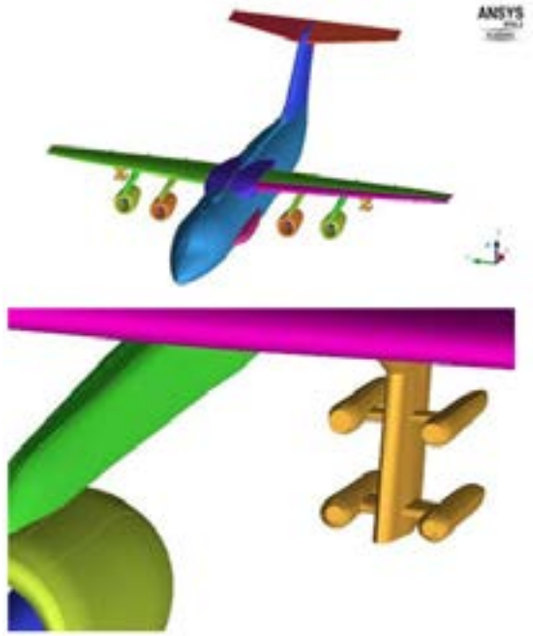

Figure 11. BAE146 solid model showing underwing pods and canisters

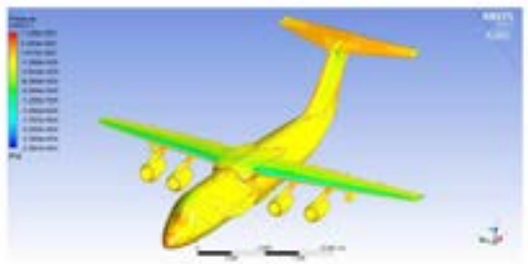

Figure 12. BAE146 pressure field at science speed (6o angle of attack and 107m/s, ISA SL)

Flow solutions for the inviscid case at ISA sea level and test conditions with an angle of attack of 6o and a true airspeed of 107m/s (zero sideslip angle) are shown in Figures 12 - 14. Although the pressure field around the aircraft is as expected, examination of the local flow direction on the canisters shows significant deviation from freestream both with respect to the angle of attack and sideslip angle. The view from the bottom of the aircraft (see Figure 14) shows a substantial crossflow on the canisters. Analysis has found flow deviations of up to 5 degrees from probe reference lines.

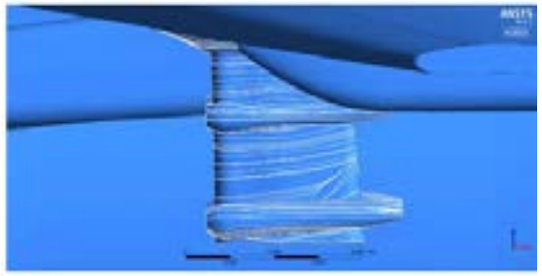

Figure 13. Surface flow visualisation of underwing pods and canisters

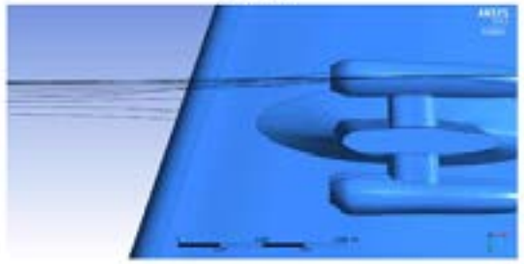

Figure 14. . Flow visualisation of underwing pods and canisters

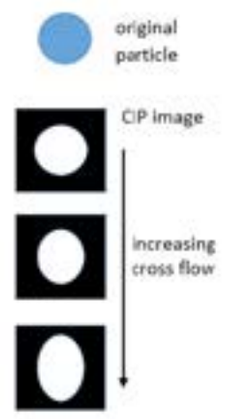

Figure 16. Effect of cross flow component on cloud imaging probe (CIP) liquid particle image

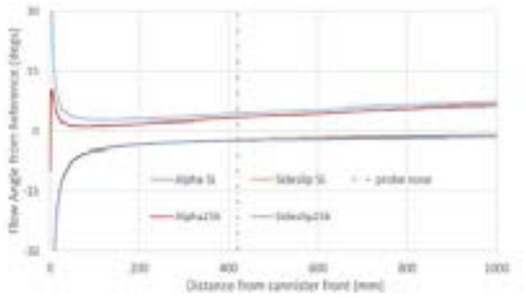

Figure 15. Flow angularity forward of bottom outer canister with typical instrument probe nose position

Such flow deviations from the probe reference lines and the associated cross-flows adjacent to the probes can induce errors in the measurements from the probes. As an example, a cloud imaging probe (CIP) on the aircraft uses instantaneous profile images of the particles through the probe volume, to estimate particle size. Cross flows into the probe measurement volume will distort the particle shape as they pass through the imaging volume (see Figure 16). Liquid particles in clouds which may start as a spheroids in the freestream will be distorted into an ellipsoid. Depending on the probe algorithm, this distortion will induce an error in the size estimation. Figure 17 confirms this crossflow effect on particle size from real airborne data taken from the FAAM aircraft in a recent flight test campaign. The probe is a model DMT CIP100-2. Therefore in certain measurement scenarios, the CFD data will allow a correction to be developed for these types of measurements.

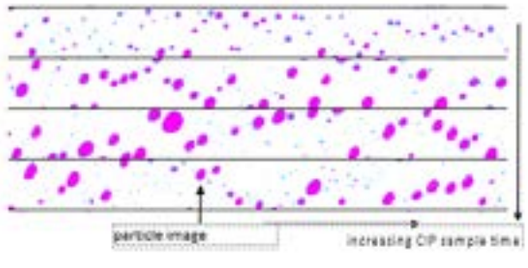

Figure 17. CIP image sequence from the Facility for Airborne Atmospheric Measurements (FAAM) at science speed (courtesy G. Nott and C. Reed, FAAM)

VI. ADVANCED MEASUREMENT SENSORS

Fibre optic sensors are now mature enough to allow their application in aerospace environments (Lawson et al 2016, Lawson et al 2017, Bennett and Lawson 2018). In particular, interrogators which are aerospace approved, for example which meet a Mil Std or CS-25, offer new opportunities to test fibre optic sensors in flight. Recent work by Cranfield University has proven pressure and strain measurement by using a Bulldog aerobatic light aircraft (see Figure 18). The basic sensor suite is shown in Figure 19 and a sample of data taken during an aerobatic manoeuvre shows the response of the sensor under high normal g-loads (see Figure 20). The key challenges in the current sensor designs are removing temperature sensitivity from the system, particularly for the pressure sensors, which are based on Fabry Perot methods.

Potentially these sensors can be integrated into more advanced aircraft composite structures, to offer real time monitoring of structure characteristics, including shape and also health monitoring for longer term analysis of the

structure. Future advances in pressure sensors, in addition, offer the potential for control flow on the aircraft.

sensor path length to resolution or signal to noise, therefore allowing multiple sensors to be placed over a large structure, without degradation of sensor performance.

Work continues at Cranfield University in this area of instrumentation development, with a potential flight test of fibre sensors on a CS-25 category aircraft expected in the next 2 years.

Figure 18. Cranfield University Bulldog airborne test platform

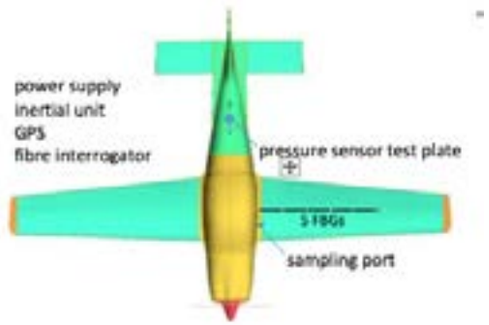

Figure 19. Cranfield University Bulldog overview of advanced instrumentation suite

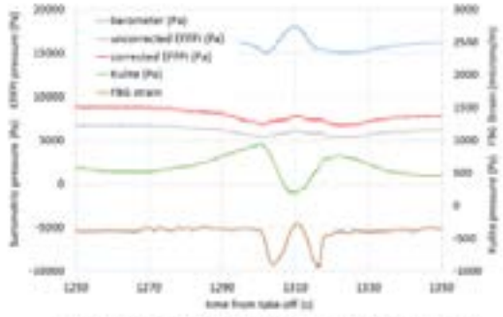

Figure 20. Flight test fibre optic data taken during an aerobatic manoeuvre in the Bulldog aircraft

The flow chart in Figure 21 gives a summary of fibre optic sensors systems which can be combined to study parameters ranging from temperature to shape. In general, Fabry Perot sensors are adapted to measure pressure, fibre Bragg gratings (FBGs) measure strain and fibre segment interferometry (FSI) measures displacement. In the latter two cases, these measurand can be used to estimate object shape such as for a wing in flight. A major advantage of these sensors is also immunity from electromagnetic interference and virtual independence of

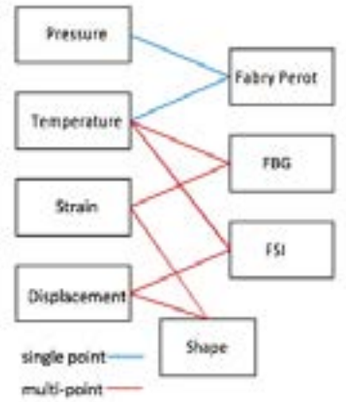

Figure 21. Fibre optic sensor measurands and methods

VII. CONCLUSIONS

This paper has presented examples of new approaches to develop and refine sensors and instruments for use in airborne test. The application of computational fluid dynamics (CFD), combined with detailed solid models of the aircraft, now offer the potential to optimise instruments and sensors on the aircraft, ahead of any airborne test. These methods can also be retrospectively applied to an aircraft to improve or offer correction methods to the sensors and instruments, thus reducing instrument error and increasing instrumental and sensor performance.

Examples of advanced fibre optic sensors for airborne test have also been presented and their advantages discussed. This technology is now mature enough to give detailed and integrated measurements in airborne test and future aircraft designs.

VIII. REFERENCES

Anderson JD (1995), Computational Fluid Dynamics: the basics with applications. McGraw-Hill International Editions.

Bennett CJ & Lawson NJ (2018) On the development of flight-test equipment in relation to the aircraft spin, Progress in Aerospace Sciences, Early online.

Bennett CJ, Lawson NJ, Gautrey JE & Cooke A (2017a) CFD Simulation of flow around angle of attack and sideslip angle vanes on a BAe Jetstream 3102 - Part 1, Aerospace Science and Technology, 68 (September) 561-576.

Bennett CJ, Lawson NJ, Gautrey JE & Cooke A (2017b) CFD Simulation of flow around angle of attack and sideslip angle vanes on a BAe Jetstream 3102 - Part 2, Aerospace Science and Technology, 68 (September) 577-587.

Boden F, Lawson N, Jentik HW, Kompenhams J (2013) Advanced In-Flight Measurement Techniques, Springer-Verlag, Berlin. Jameson A and Ou K (2011) 50 Years of Transonic Aircraft Design. Progress in Aerospace Sciences, Vol 47, pp 308-318.

Kissinger T, Chehura E, Staines SE, James SW & Tatam RP (2018) Dynamic fiber-optic shape sensing using fiber segment interferometry, Journal of Lightwave Technology, 36 (4) 917-925. Lawson NJ, Correia R, James SW, Gautrey, JE, Invers Rubio G, Staines SE, Partridge M & Tatam RP (2017) Development of the Cranfield University Bulldog flight test facility, Aeronautical Journal -New Series-, 121 (1238) 533-552.

Lawson NJ, Jacques H, Gautrey JE, Cooke AK, Holt JC & Garry KP (2017) Jetstream 31 National Flying Laboratory: Lift and drag measurement and modelling, Aerospace Science and Technology, 60 84-95.

Lawson NJ, Correia R, James SW, Partridge M, Staines SE, Gautrey JE, Garry KP, Holt JC & Tatam RP (2016) Development and application of optical fibre strain and pressure sensors for in-flight measurements, Measurement Science and Technology, 27 (10).

Lawson NJ, Gautrey JE, Salmon N, Garry KP & Pintiau A (2014) Modelling of a Scottish Aviation Bulldog using reverse engineering, wind tunnel and numerical methods, Proceedings of the Institution of Mechanical Engineers, Part G: Journal of Aerospace Engineering, 228 (14) 2736-2742.

Lawson NJ, Salmon N, Gautrey JE & Bailey R (2013) Comparison of flight test data with a computational fluid dynamics model of a Scottish Aviation Bulldog aircraft, Aeronautical Journal -New Series-, 117 (1198) 1273-1291.

McBeath K (2014) The use of aircraft for meteorological research in the United Kingdom, Meteorol. Appl. 21: 105–116

Rao YJ (2006) Recent progress in fibre-optic extrinsic Fabry-Perot interferometric sensors, Optical Fibre Tech., 12(3), pp. 227-237. Rao YJ (1999) Recent progress in applications of in-fibre Bragg grating sensors, Opt. Laser. Eng., 31, pp. 297-324.

Rawlings K (1981) A method for estimating upwash angle at noseboom-mounted vanes, USAF Report AFFTC-TIM-81-1 Reasor DA Jr., Bhamidipat KKi, and Woolf RK (2015) Numerical Predictions of Static-Pressure-Error Corrections for a Modified T-38C Aircraft, Journal of Aircraft, Vol. 52, No. 4, pp. 1326-1335. van der Linden JC. and Mensink HA (1977) Linear and Angular Measurement of Aircraft Components, AGARD and RTO Flight Test Instrumentation Series AGARDograph 160 (AG 160), Volume 8.

Wuest W (1980) Pressure and Flow Measurement, AGARD and RTO Flight Test Instrumentation Series AGARDograph 160 (AG 160), Volume 8.

ACKNOWLEDGEMENT

The author would like to acknowledge Dr Chris Bennett (Cranfield University), Dr Graeme Nott and Chris Reed (Facility for Airborne Atmospheric Measurements)